



Highly effective removal of Pb^{2+} in aqueous solution by Na-X zeolite derived from coal gangue

Qilong Ge^{1,2} · Muhammad Moeen¹ · Qi Tian^{1,3} · Jianjie Xu¹ · Kaiqing Feng¹

Received: 31 October 2019 / Accepted: 16 December 2019 / Published online: 28 December 2019
© Springer-Verlag GmbH Germany, part of Springer Nature 2019

Abstract

The present study aimed to synthesize Na-X zeolite from coal gangue powder (CGP) via the alkali fusion hydrothermal method. The optimal synthetic conditions were investigated, the mass ratio of CGP/NaOH(s) was 1:1.25, and crystallization reaction time was 12 h. X-ray powder diffraction, scanning electron microscopy energy-dispersive X-ray spectrum, and Fourier transform infrared spectrometer techniques were used to test the properties of resultant zeolite product, which was highly identical to that of commercial zeolite. The efficiencies of the synthetic zeolite for Pb^{2+} adsorption were analyzed on factors including solution pH, adsorbent dosage, temperature, and contact time. Compared with the pseudo-first-order, Elovich, Freundlich, and Temkin models, the pseudo-second-order and Langmuir models were fitted more satisfactorily with the dynamic data and adsorption equilibrium data, respectively. The maximum Pb^{2+} adsorption capacity of synthetic zeolite (457 mg/g) could be reached when the pH, contact time, temperature, and initial Pb^{2+} concentration was 6, 40 min, 45 °C, and 200 mg/L. The adsorption capacity was higher than many of the natural and synthetic zeolites reported in previous literature.

Keywords Coal gangue · Na-X zeolite · NaOH · The hydrothermal method · Pb^{2+} adsorption

Abbreviations

CGP	Coal gangue powder
XRF	X-ray fluorescence
XRD	X-ray diffraction
SEM	Scanning electron microscopy
EDS	Energy-dispersive X-ray spectroscopy
FTIR	Fourier transform infrared
FAAS	Flame atomic adsorption spectrophotometer
LOI	Loss on ignition

Introduction

Lead (II) (Pb^{2+}), one of the toxic heavy metal pollutants, is released into the environment, including soil, surface water, and groundwater (Ibrahim et al. 2010). The sources of lead pollution include discarded batteries, painting materials, and lead-containing pesticides (Barbosa et al. 2014). Lead is non degradable and detrimental to living beings, uniquely human (Zanin et al. 2016). For instance, it can interfere with hemoglobin synthesis, causing intellectual impairments (Gassowska et al. 2016). Many methods have been applied to remove Pb^{2+} mainly from aqueous solution, including solvent extraction, micro-biological degradation, reverse osmosis, electro-dialysis, and adsorption (Al-Harashsheh et al. 2015). Remediation through the adsorption method is one of the most effective techniques among these methods. It is imperative to select a suitable adsorbent for large-scale application, considering the cost and efficiency. Low-cost and high-efficient adsorbents are always preferred (Bortone et al. 2013).

Coal gangue is a hazardous and complex solid by-product produced in the coal mining and washing process, being one of the most significant industrial residues. The average production of coal gangue is about 15% of total coal production,

Responsible editor: Tito Roberto Cadaval Jr

✉ Qi Tian
tqytut@163.com

¹ College of Environmental Science and Engineering, Taiyuan University of Technology, Taiyuan 030024, China

² Department of Environmental Science and Engineering, Taiyuan College, Taiyuan 030032, China

³ College of Civil Engineering, Taiyuan University of Technology, Taiyuan 030024, China

and almost 27% of the world's energy consumption is from coal combustion (Qin and Gao 2019; Bhuiyan et al. 2010).

The massive accumulation and improper disposal of coal gangue pose many harmful effects on the ecological environment, such as polluted water, soil, and atmosphere (Haibin and Zhenling 2010; Liu et al. 2020). The disposal of such a large amount of coal gangue efficiently is a worldwide severe and meaningful problem, especially for China, because China contributes 50.72% of the total world coal consumption in 2017 (Li and Wang 2019). However, the utilization rate of coal gangue is still lower, although researches have been done to investigate the reuse of coal gangue. For instance, in China, the overall utilization rate of coal gangue is 64% in 2014, and they were mainly used to yield building material and generate electricity (Wang et al. 2016; Zhou et al. 2014).

Coal gangue contains a large quantity of Si and Al, which has the potential to be used in the synthesis of zeolite, one of the high-value-added inorganic porous materials (Gao et al. 2015). Above all, the Si/Al molar ratio in coal gangue is usually from 1 to 2, which is quite close to the Si/Al molar ratio in faujasite zeolite and divided into two types. Both of them have the same crystal structure but the different chemical composition, namely Na-X zeolite with Si/Al = 1.0–1.5 and Na-Y zeolite with Si/Al = 1.5–3.0 (Zhang et al. 2013). So coal gangue can be viewed as the primary industrial raw material to synthesize zeolite. Besides, various techniques, such as ultrasonic or microwave-assisted technique, hydrothermal treatment, and in-situ crystallization technique, have been used to prepare zeolite from fly ash (Sivalingam and Sen 2018; Miyake et al. 2008; Wei et al. 2019; Aldahri et al. 2016). Among these methods, melting hydrothermal synthesis is a conventional and mature technique that has excellent potential for the product on a large scale (Murayama et al. 2002). As OH⁻ produced by NaOH solution weakens the binding between SiO₂ and Al₂O₃ in the kaolinite of coal gangue and destroy the bond structures of SiO₂ and Al₂O₃, causing thermodynamically unstable states, which induce soluble amorphous Si and Al (Yang et al. 2019a, b). It is also noted that Na⁺ has positive influences on the crystallization and nucleation during the zeolite synthesis process (Doyle et al. 2017). Although several studies have reported about the preparation zeolite from coal gangue, most of the final products are always A-type zeolite (Qian and Li 2015; Zhou et al. 2020). Very few researches consider the synthesis of Na-X zeolite from coal gangue with a convenient and straightforward method and evaluation of synthetic zeolite in the application.

These are the defects that prevent practical large-scale zeolite synthesis via conventional hydrothermal route. Due to this background, the primary purpose of this study was to activate coal gangue using moderate NaOH(s) followed by the hydrothermal route to synthesize zeolite from coal gangue. Therefore, the main objectives of the present study are (1) A simple technique of synthetic Na-X zeolite using coal gangue

as a raw material without calcination-pickling pretreatment was revealed; (2) optimum synthesis conditions of pure and single-phase Na-X zeolite were determined; (3) the synthetic zeolite is characterized using XRF, XRD, SEM, and FTIR techniques; (4) the performance of synthetic zeolite for the adsorption of Pb²⁺ in aqueous solution was investigated. This work is conducive to the recycling of mining solid waste.

Material and methods

Coal gangue and chemicals

The raw coal gangue used in this experiment was obtained from the Longquan coal mine in Loufan County, Shanxi Province, China. All chemical reagents (e.g., NaOH and Pb(NO₃)₂) purchased from the Tianjin Hengxing Chemical Preparation Corporation were analytical grade. The purity levels of the analytical grade NaOH and Pb(NO₃)₂ are 96% and 99%, respectively. Among them, Pb(NO₃)₂ was used for the adsorption experiment. NaOH was used to synthesize zeolite. Deionized water with a conductivity of 2.7 μs/cm was used in this study.

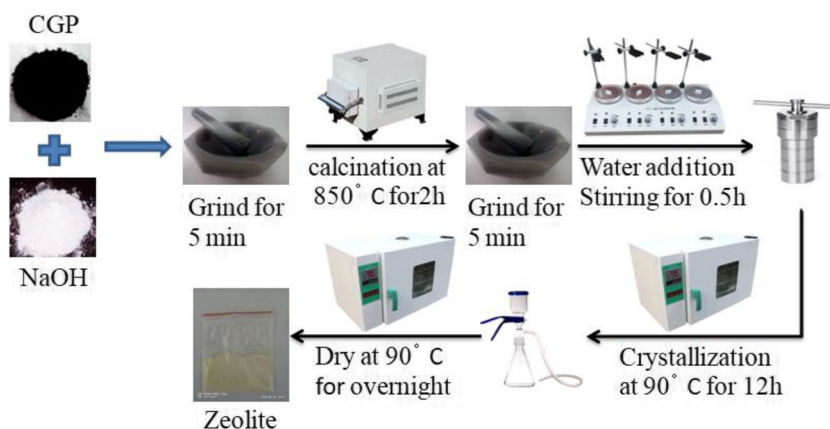
Preparation of Na-X zeolite

The raw coal gangue samples were crushed into different particle sizes. Then, they were milled and passed through a 150-mesh sieve to gain the coal gangue powder (CGP) for the next step. Subsequently, the 2 g CGP was mixed and ground with a certain mass of NaOH(s) in a mortar for 5 min to obtain a homogeneous mixture. After that, the homogeneous mixture was packed in the crucible and placed in the muffle furnace under an air atmosphere at 850 °C for 2 h to activate CGP and remove unburned carbon. After being cooled to room temperature, the fused samples were placed into the mortar, ground into powder, dissolved with 15 mL deionized water, stirred for 0.5 h, and then crystallized in a hot air oven at 90 °C for 4, 8, 12, and 24 h, respectively. The product was separated through vacuum filtration with deionized water several times until the pH reached 8, dried 105 °C for 6 h before characterization and adsorption experiment. Figure 1 shows the detailed process.

Material characterization

The chemical composition of CGP and zeolite samples was examined by X-ray fluorescence analyzer spectrometer (XRF). The identification of CGP and zeolite product was checked by power X-ray diffraction (XRD) with Cu Kα radiation generated at 40 kV and 40 mA. The functional groups of the samples were determined by Fourier transform infrared spectroscopy (FTIR) using

Fig. 1 Process for Na-X zeolite synthesis from coal gangue



the standard KBr disk method, the microstructure and morphology of CGP, and zeolite samples were examined by scanning electron microscopy and energy-dispersive X-ray spectroscopy (SEM-EDS). The flame atomic absorption spectrophotometer (FAAS) was used to determine the Pb^{2+} concentration.

Pb^{2+} adsorption experiments

Pb^{2+} solution was prepared by dissolving lead nitrate in deionized water. Then, the influence of pH value on the Pb^{2+} adsorption was investigated in the range of 2–8 by adding appropriate 0.01 M HNO_3 or 0.01 M $NaOH$ solution. 0.02 g Na-X zeolite powder was added to 150 mL Erlenmeyer flasks with 50 mL Pb^{2+} solution, sealed and shaken at 160 rpm for 40 min. To investigate the influence adsorbent addition and temperature, various dosage (0.0025, 0.005, 0.010, 0.015, 0.020, 0.025, and 0.030 g) were added into the Pb^{2+} solution shaken at different temperature (25, 35, and 45 °C), respectively, shaking at 160 rpm and pH=6 for 40 min. To determine the effect of contact time on the Pb^{2+} adsorption, the experiment was kept at 160 rpm, 45 °C, and pH=6 with the varying time periods (5, 10, 15, 20, 30, 40, 50, 60 min). The solution was collected and centrifuged at 8000 rpm for 10 min after the reaction. Residual Pb^{2+} concentration was detected by the flame atomic absorption spectrophotometer (FAAS).

The Pb^{2+} adsorption capacity was calculated by Eq. (1):

$$q_e = \frac{(C_0 - C_e)V}{m} \quad (1)$$

In which, q_e (mg/g) is the Pb^{2+} adsorption amount per unit mass of adsorbent. C_0 (mg/L) and C_e (mg/L) represent the initial and equilibrium Pb^{2+} concentration in solution, respectively. V (L) denotes the solution volume, and m (g) stand for the mass of adsorbent. All experiments were performed in duplicate.

Results and discussion

Composition analysis of CGP and synthetic zeolite

As shown in Table 1, the CGP used in this study is mainly composed of 60.52 wt.% SiO_2 and 33.02 wt.% Al_2O_3 . This CGP is different from other coal gangue because it has a high content of silicon and alumina (more than 90 % of SiO_2 and Al_2O_3) (Doyle et al. 2017; Zhou et al. 2020). There is only 2.09 wt% of K_2O and less than 2 wt% of Fe_2O_3 , which can be negligible. Other contents such as CaO and TiO_2 are almost zero. SiO_2/Al_2O_3 molar ratio of the coal gangue samples ($n(SiO_2)/n(Al_2O_3) = 3.1$) is close to the optimal SiO_2/Al_2O_3 molar ratio of the reaction mixture ($n(SiO_2/Al_2O_3) = 2.9$) (Yang et al. 2019a, b). That is to say, Al_2O_3 and SiO_2 that can provide aluminum and silicon sources respectively in coal gangue are the primary raw materials for zeolite synthesis. The Na-X zeolite synthesis here was obtained at 90 °C because the high crystallization temperature generally results in hydroxyl sodalite development and energy consumption (Qian and Li 2015).

Based on the results of the XRD pattern (Fig. 2(a)) of CGP, the predominated mineral phase of coal gangue is kaolinite and silicon dioxide. The SEM image (Fig. 2(b)) illustrated in the surface of raw coal gangue is blocky, dense, and blurred. EDS demonstrates that the contents of Al and Si were high, which is consistent with the results of the XRF mentioned above.

Na-X zeolite obtained here at 90 °C and CGP/ $NaOH(s) = 1.25$ for 12 h contains SiO_2 48.73%, Al_2O_3 28.57%, and Na_2O 18.97%. It shows Na:Al:Si molar ratio of 1.09:1:1.45, which

Table 1 Chemical composition of CGP and synthetic Na-X zeolite by XRF (% w) LOI loss on ignition

Sample	SiO_2	Al_2O_3	Fe_2O_3	Na_2O	CaO	TiO_2	K_2O	LOI
CGP	60.52	33.02	1.73	<0.1	0.42	1.03	2.09	20.7
Na-X zeolite	48.73	28.57	1.57	18.97	0.41	0.73	0.77	18.3

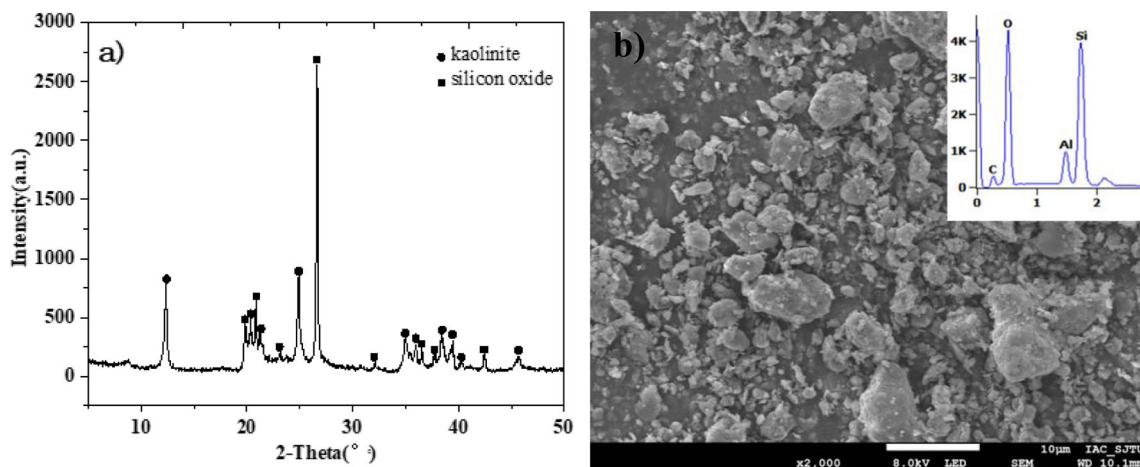


Fig. 2 (a) XRD pattern of CGP. (b) SEM image and EDS analysis of CGP

is close to the molar ratio of the theoretical formula ($\text{Na}_2\text{Al}_2\text{Si}_{3.3}\text{O}_{10.6}\cdot 7\text{H}_2\text{O}$, as identified in Fig. 3).

Effect of CGP to NaOH(s) mass ratio

To scientifically investigate the effect of alkalinity, Fig. 3 exhibits the XRD patterns of the synthetic product using different CGP/NaOH(s) mixing ratio (1:1.1, 1:1.25, 1:1.4, 1:1.55), a critical factor for the zeolite synthesis. Other influence factors remain unchanged. The XRD patterns of synthetic zeolite illustrate peaks at the ranges of $2\theta = 6.2^\circ, 15.5^\circ, 23.4^\circ, 26.8^\circ, 31.2^\circ$, which correspond to the diffraction peaks of standard JCPDS card 12-0228 (Reinoso et al. 2018). It can be observed from Fig. 3(a) the mixture powder still exist amorphous status when the NaOH(s) content is relatively low, because NaOH provides insufficient amounts of OH^- for CGP activation and hydrothermal reaction (Murayama et al. 2002). As the ratio increase, amorphous status disappears. However, some peaks

corresponding to Na-A zeolite can be seen from Fig. 3(d). So it is necessary to keep the amount of the NaOH(s) at appropriate ratio since low NaOH content is not beneficial to the crystallization, while high content can promote the formation of other kind of zeolite (Liu et al. 2013). The optimal mixing ratio should be controlled at about 1:1.25 to achieve the high purity Na-X zeolite in the following study.

Effect of crystallization time

XRD patterns of Na-X zeolite synthesized at various crystallization times (4, 8, 12, and 24 h) at 90°C are presented in Fig. 4(a–d), respectively. Very weak peaks of Na-X zeolite in Fig. 4(a) at 4 h show that the zeolite phase began to appear. With the increase of crystallization time (from 4 to 24 h), Na-X zeolites became the predominated crystalline phase and the XRD intensities of them also improved, which is consistent with other literatures (Yang et al. 2019a, b; Lee et al. 2018; Wang et al. 2008). This finding suggests that it is necessary to extend crystallization time for the aim of preparing the high

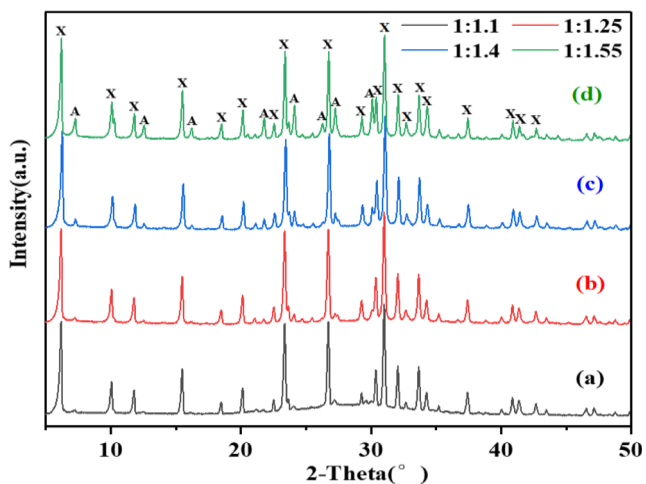


Fig. 3 XRD patterns of the products prepared under different CGP/NaOH mass ratio: 1:1.1 (a), 1:1.25 (b), 1:1.4 (c) and 1:1.55 (d). The letters A and X represent the characteristic peaks of Na-A and Na-X zeolite, respectively

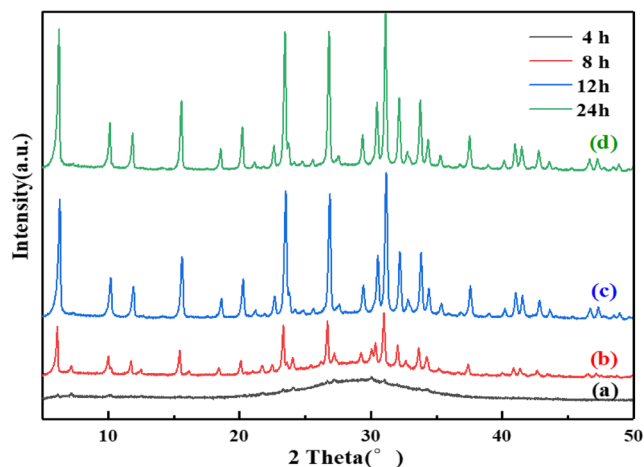


Fig. 4 XRD patterns of zeolite synthesized at different crystallization time: 4h (a), 8h (b), 12h (c) and 24h (d)

specific surface area and good crystallized Na-X zeolite. Moreover, compared with XRD pattern of Na-X synthesized at crystalline time 12 h (Fig. 4(c)), as the crystalline time extended to 24 h (Fig. 4(d)), diffraction peaks changed very slightly. Hence, considering the economical requirement and technical requirement, the optimal crystalline time was controlled at 12 h.

Comparison with commercial Na-X zeolite

SEM analysis

The corresponding SEM micrographs of Na-X zeolite synthesized at different reaction times and commercial-grade zeolite are illustrated in Fig. 5(a–f). When the crystallization time was too short such as 4 h (Fig. 5(a)) and 8 h (Fig. 5(b)), the poorly developed Na-X zeolite would be obtained probably because the amorphous silicon-aluminum gel components dispersed in the hydrothermal system dominated. Figure 5(c) and (f) show particle size for synthetic and commercial zeolite particles are about 12–17 μm and 2 μm , respectively. As the synthetic reaction time extended, the particle size enlarged. Octahedron particles were well homodispersed and predominate in the final products (Fig. 5(c), (d)). Figure 5(e) represents a high-power microscope image of the synthetic Na-X zeolite at crystallization 12 h, which presents more regular and distinct pyramidal octahedron structures.

FTIR analysis

The FTIR spectra of the commercial-grade and synthetic zeolite under the optimal artificial conditions (CGP/NaOH(s)) = 1:1.25, crystalline time = 12 h) is presented in Fig. 6. Both of them have almost identical transmittance peaks, which mean functional groups are the same in both samples. In this study, narrow bands centered at 977.73 cm^{-1} and 1644.38 cm^{-1} were attributed to Si-OH and H-OH bands, respectively (Reynolds et al. 2001; Liu et al. 2016). The group near 565.04 cm^{-1} was considered as the Al-OH stretch vibration (Liu et al. 2010). The peak occurred at 755.69 cm^{-1} was ascribed to the stretching modes of tetrahedral atoms (Nekhunguni et al. 2017). The influential bands at 671.1 cm^{-1} and 462.83 cm^{-1} were assigned to the symmetric stretching vibration and bending vibration modes of Si-O or Al-O bands, respectively, which was matched with commercial-grade zeolite very well (Faghihian et al. 2012). Besides, the broadband at 3467.38 cm^{-1} confirmed the stretching mode of hydrogen-bonded OH (Ojha et al. 2004). Therefore, the results of XRD, SEM, and FTIR indicate that the CGP is successfully and efficiently converted into Na-X zeolite.

Pb²⁺ adsorption experiment

Pb²⁺ adsorption by the prepared zeolite with different initial pH is detected in Fig. 7. It can be observed that as pH increases from 2 to 6, Pb²⁺ adsorption capacity rises. Subsequently, it

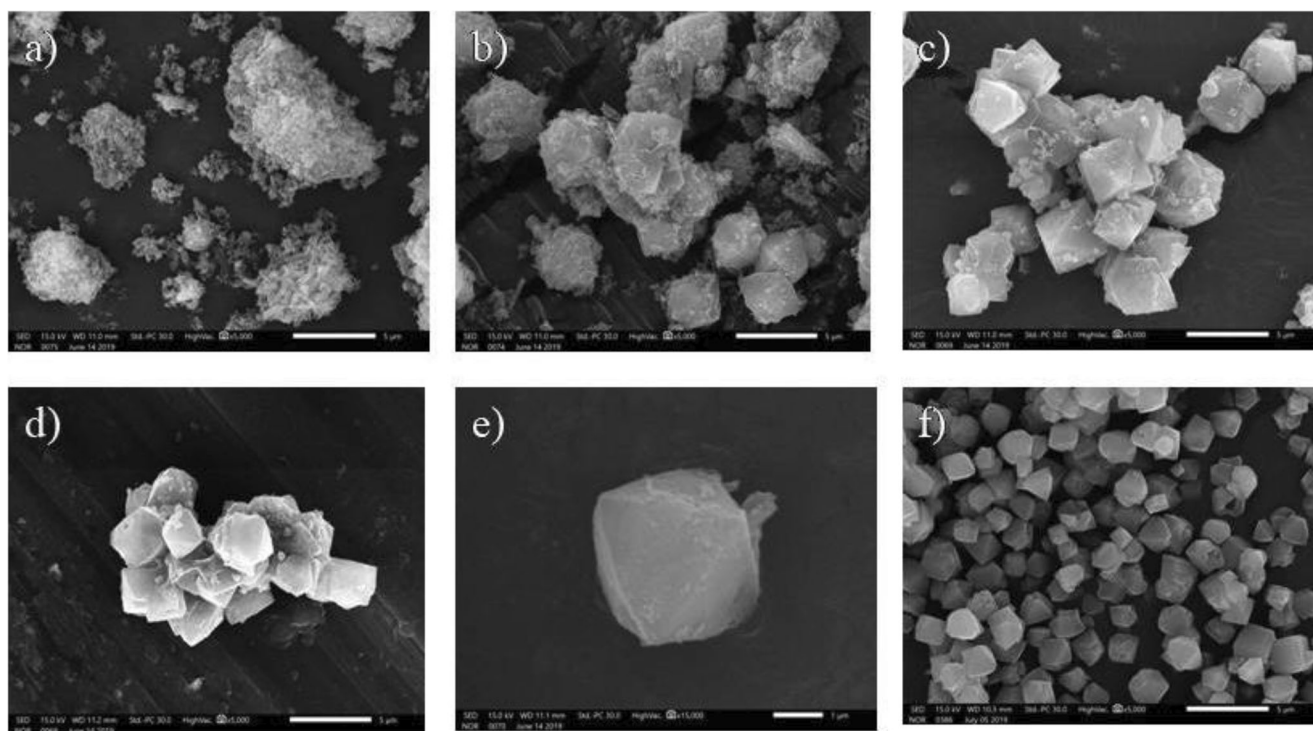


Fig. 5 SEM images of the synthetic Na-X zeolite at crystallization time 4h (a), 8h (b), 12h (c), 24h (d), the high power microscope image of the synthetic Na-X zeolite at crystallization time 12h (e) and commercial grade zeolite (f)

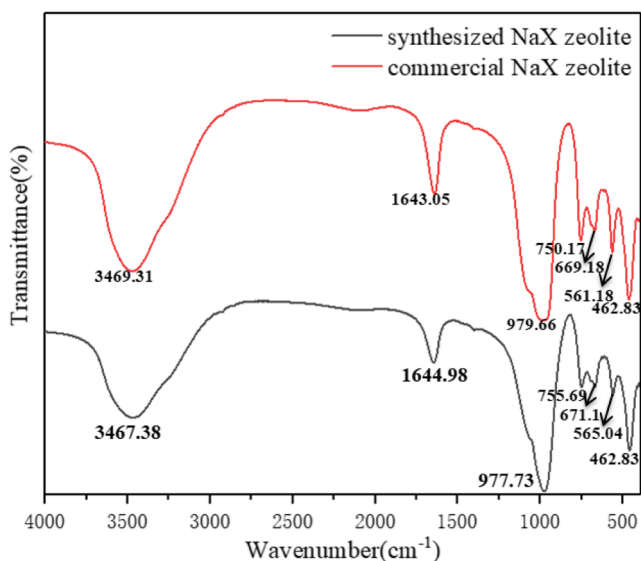


Fig. 6 Infrared analysis of commercial and synthetic zeolite

decreases slightly at pH = 7 and 8. Hence, the maximum Pb^{2+} adsorption capacity occurs at pH = 6. This finding agrees well with that reported by Pankaj K. et al. which showed that the highest Pb^{2+} adsorption capacity of Na-X zeolite could be achieved at the pH = 6 (Pandey et al. 2015). Our finding also matches well with Zahra Shariatinia et al., who found that the modified Na-Y zeolite adsorption could be more selective for Pb^{2+} at pH = 6 (Shariatinia et al. 2018). Because there is a competition between H_3O^+ and Pb^{2+} in the solution at pH below 6, which limited exchange sites of synthetic zeolite (Murayama et al. 2002). Especially under strong acid condition (pH = 2), more positive H_3O^+ species are available. The performance of Pb^{2+} adsorption capacity is very poor (only 56.87 mg/g). When Pb^{2+} cations predominate in the solution at pH of 3–6, Pb^{2+} is drastically adsorbed as result of the surface hydroxyl groups generated by the zeolite surface with water could neutralize the H_3O^+ (Liu et al. 2018). Moreover, at pH above 7, the mild decline is probably due to the increase of $Pb(OH)_2$ that cannot enter in zeolite by ion exchange.

To enhance the interactions between Pb^{2+} and adsorption sites of zeolite products, optimum additional dosage and temperature were investigated. Figure 7 (b) illustrates that Pb^{2+} removal is promoted with the increase of adsorbent dosage from 0.0025 to 0.02. However, further rising the adsorption dose to 0.025 g or 0.03 g results in a slight rise in the Pb^{2+} removal. So it is almost constant, and the adsorption dose of 0.02 g is consequently chosen as optimization. Besides, as the temperature rises from 25 to 45 °C, the Pb^{2+} adsorption capacity on synthetic zeolite also increases. Due to that, this process is endothermic adsorb sites and ions exchange can be promoted by higher temperatures (Liu et al. 2018; Shariatinia and Bagherpour 2018). To evaluate the effect of adsorption time on the Pb^{2+} removal, 0.02 g of zeolite was used to identify the

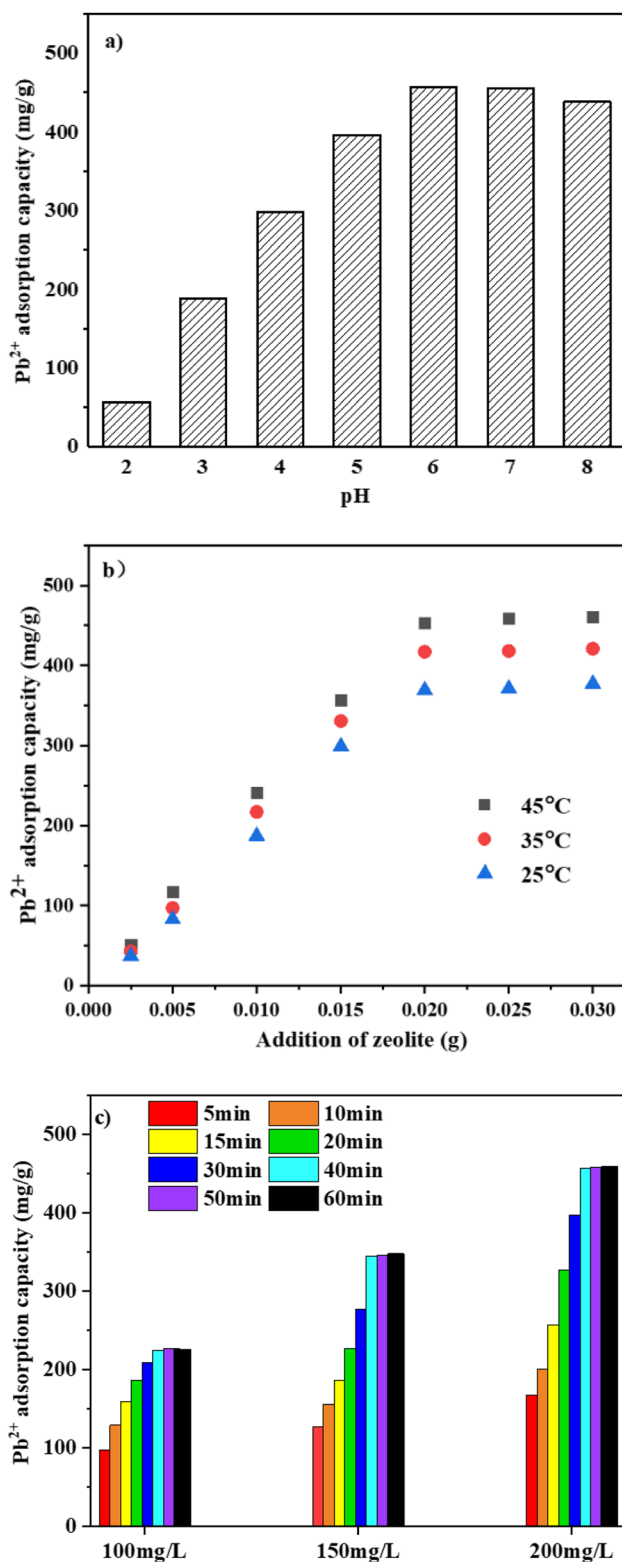


Fig. 7 The influence of pH (a), adsorbent dosage (b), temperature (b), and contact time (c) on the Pb^{2+} removal using synthetic zeolite

best condition for this factor at pH = 6.0. It is found from Fig. 7c that Pb^{2+} adsorption capacity can be enhanced by increasing the adsorption time. Besides, after 40 min, the

Pb²⁺ removal becomes approximately constant, which indicate 40 min is the optimum adsorption time.

It is worth noting that although the increase of contact time or zeolite dose could continually promote Pb²⁺ removal, in the real application, the operating cost would be relatively high. This weakens the economic advantages of coal gangue-based zeolite. So the zeolite dose and adsorption time should be set based on the requirement of both technology and financial. Furthermore, Because Na-X zeolite has a uniform pore size from 0.8–1.2 nm and the Pb²⁺ hydrated ionic radius is about 0.4 nm, Na-X zeolite has a high Pb²⁺ removal percentage under the specific conditions.

Adsorption kinetic study

The kinetics of Pb²⁺ adsorption can be analyzed according to pseudo-first-order, pseudo-second-order, and Elovich models. These models can be expressed by Eqs. (2)–(4) in Table 2 (Zhao et al. 2010; Liu et al. 2016), where q_e (mg/g) and q_t (mg/g) are the adsorbed amounts of Pb²⁺ at equilibrium and at any time t (min), respectively. k_1 (min⁻¹) and k_2 (g mg⁻¹ min⁻¹) donate the pseudo-first-order and the pseudo-second-order rate constant, respectively. β (g mg⁻¹) and α (mg g⁻¹ min⁻¹) are the desorption rate and initial adsorption constant, respectively. The plots and corresponding fitting nonlinear curves of three kinetic models are presented in Fig. 8 at initial Pb²⁺ concentration of 100 mg/L, 150 mg/L, and 200 mg/L. Table 5 illustrates the fitting kinetic parameters and correlation coefficient (R^2). $q_{e, cal}$ and $q_{e, exp}$ are the calculated and experimental adsorption capacity of the synthetic zeolite, respectively. The Pb²⁺ adsorption capacity of synthetic zeolite raised as adsorption time goes on. The adsorption process can be divided into an initial rapid adsorption phase and a subsequent slow phase.

The best fitting of the data with the pseudo-second-order model and higher correlation coefficient ($R^2 > 0.99$) can be

observed in Fig. 8, which confirms that the Pb²⁺ adsorption accords with the pseudo-second-order model. The R^2 (< 0.97) of the pseudo-first-order and R^2 (< 0.975) of Elovich verify these two models are kinetically unsuitable. Moreover, the experimental value of $q_{e, exp}$ is closer to the calculated value of $q_{e, cal}$ by the pseudo-second-order model than using the pseudo-first-order and Elovich model. Similar results are found for Pb²⁺ adsorption by other synthetic and natural zeolites in previous literature (Ren et al. 2016; Alijani and Shariatnia 2017). Hence, it can be concluded that the kinetic Pb²⁺ adsorption mechanism of Na-X zeolite is well described by pseudo-second-order model, suggesting that chemisorptions by ion exchange, surface complexation, and(or) precipitation predominate the adsorption of Pb²⁺ onto this adsorbent. The chemical reaction is the rate-controlling step. Adsorption efficiency depends strongly on the number of active sites on the adsorbent (Alijani and Shariatnia 2017; Li et al. 2016).

Adsorption isotherms

To recognize the sorption mechanism, adsorbent affinity and its surface properties are decided by the adsorption equilibrium isotherm constants (Li et al. 2016). Figure 9 and Table 3 illustrate the adsorption isotherms of Pb²⁺ and the experimental fitting results, respectively. It can be noticed that synthetic zeolite obtained from coal gangue has a high Pb²⁺ adsorption efficiency. Hence, nonlinear equations of Langmuir, Freundlich, and Temkin isotherm models are demonstrated, respectively in Eqs. (5)–(7), where q_e , C_e , q_m , and K_L are the Pb²⁺ amount adsorbed at equilibrium (mg/g), the equilibrium concentration (mg/L), the maximum adsorption capacity (mg/g), and Langmuir equilibrium constant, respectively; K_F and n stand for the Freundlich equilibrium continuous and adsorption strength endless, respectively (Alijani et al. 2015; Alijani et al. 2014); respectively. $B = RT/b_T$, where b_T is the Temkin constant related to the heat of adsorption (J mol⁻¹), K_T is the

Table 2 Kinetics models and their parameters for the Pb²⁺ removal

Kinetics model	Linear equation	Number	Parameter	Pb ²⁺ concentration		
				100 mg/L	150 mg/L	200 mg/L
Pseudo-first-order model	$q_t = q_e(1 - e^{-k_1 t})$	(2)	$q_{e, exp}$ (mg/g)	227	345	457
			k_1 (min ⁻¹)	0.560	0.519	0.603
			$q_{e, cal}$ (mg/g)	212.1	326.7	434.1
			R^2	0.967	0.963	0.961
Pseudo-second-order model	$q_t = \frac{k_2 q_e^2 t}{1 + k_2 q_e t}$	(3)	k_2 (g/(mg min))	0.00421	0.00271	0.00227
			$q_{e, cal}$ (mg/g)	220.1	348.0	462.5
			R^2	0.991	0.994	0.992
			α (mg·g ⁻¹ min ⁻¹)	2060.9	6289.0	2541.1
Elovich model	$q_t = \frac{1}{\beta} \ln(\beta \alpha t + 1)$	(4)	β (g·mg ⁻¹)	0.0331	0.0173	0.0209
			R^2	0.972	0.968	0.961

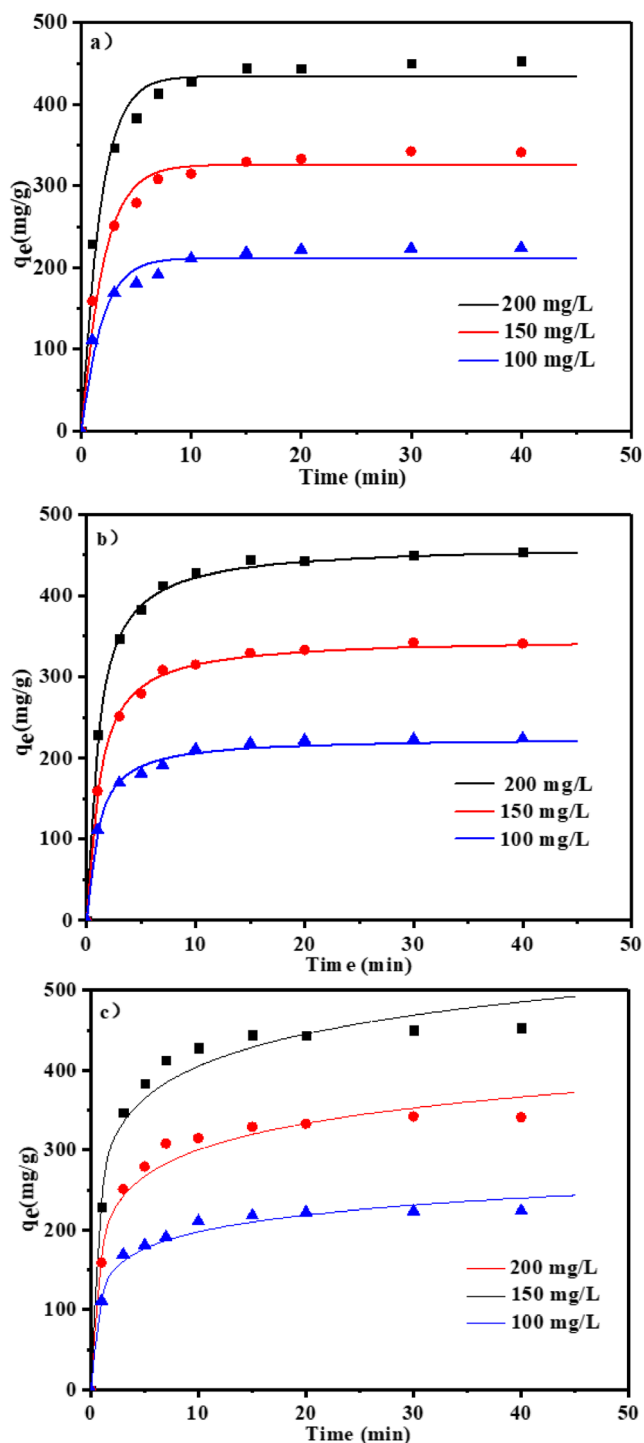


Fig. 8 The pseudo-first-order (a), pseudo-second-order (b), and Elovich (c) kinetic models for the Pb^{2+} adsorption

Temkin isotherm equilibrium binding constant ($L\ g^{-1}$), R is the ideal gas constant ($8.314\ J/(mol\ K)$). T is the absolute temperature in Kelvin.

Figure 9(a) and (b) and Table 3 demonstrated the plots, constant values, and fitting degree of Langmuir, Freundlich, and Temkin functions for Pb^{2+} adsorption, respectively. For the Langmuir model, the correlation coefficients (R^2) belong

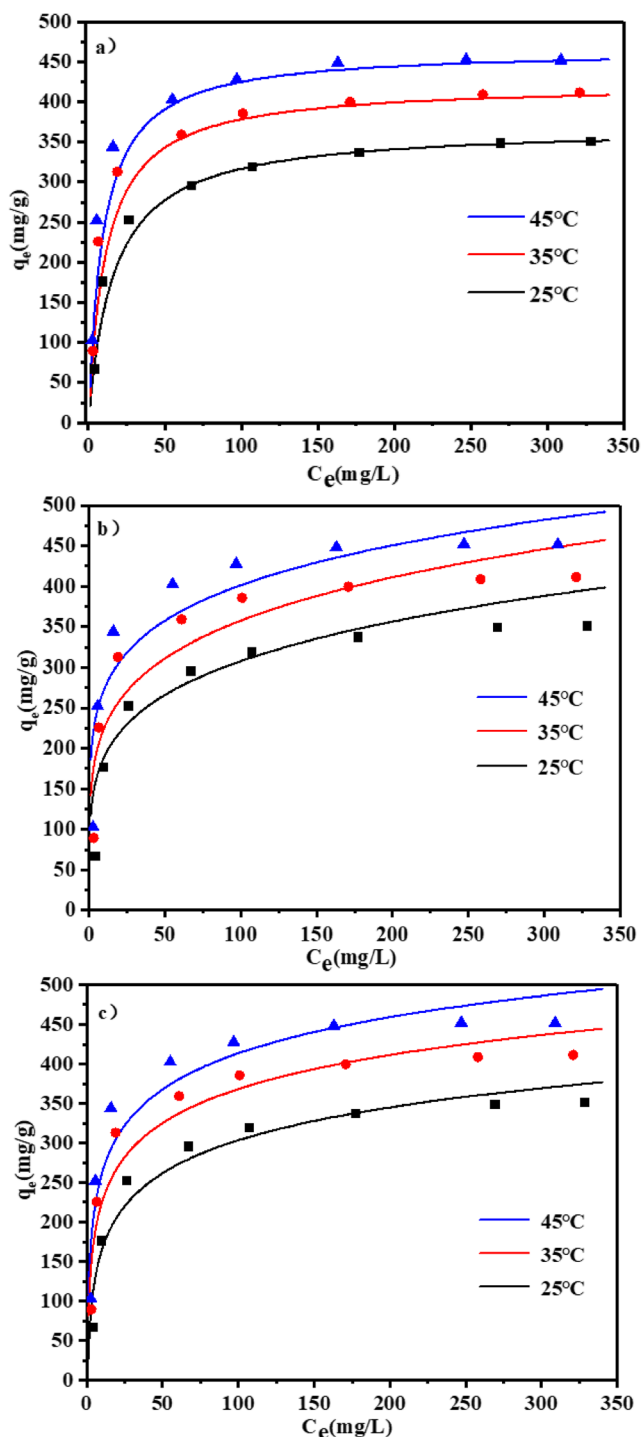


Fig. 9 Langmuir (a), Freundlich (b), and Temkin (c) for the Pb^{2+} adsorption using synthetic zeolite as adsorbents at various temperatures (25 °C, 35 °C, 45 °C, respectively)

to the range of 0.995–0.997, proving the Pb^{2+} removal accords with this isotherm model. Concerning the Freundlich and Temkin isotherm model, the R^2 is at the range of 0.82–0.87 and 0.89–0.93, respectively, which also prove that the adsorption mechanism is mainly controlled by chemical reactions. Besides, bound adsorbate molecules interact independently.

Table 3 Isotherms parameters obtained for the Pb²⁺ removal using synthetic zeolite as at various temperatures (25 °C, 35 °C, 45 °C) respectively

Isotherm model	Linear equation	Number	Parameter	Temperature 25 °C, 35 °C, 45 °C		
Langmuir	$q_e = \frac{K_L C_e q_m}{1 + K_L C_e}$	(5)	K_L	0.0604	0.0867	0.105
			q_{\max} (mg/g)	369.0	421.9	465.1
			R^2	0.995	0.995	0.997
Freundlich	$q_e = K_F C_e^{1/n}$	(6)	K_F	186.1	141.7	116.5
			$1/n$	0.167	0.201	0.211
			R^2	0.8211	0.828	0.8633
Temkin	$q_e = B \log(C_e K_T)$	(7)	K_T	5.232	3.710	1.565
			B	152.1	143.3	128.2
			R^2	0.8974	0.901	0.926

Moreover, the results show that almost all the sorption sites are equivalent, and the adsorption belongs to homogenous and monolayer (Zhang et al. 2017).

Adsorption thermodynamics

The thermodynamic parameters of Pb²⁺ adsorption on Na-X zeolite are calculated at pH = 6 at 298, 308, and 318 K. Equations (8)–(10) can express the standard Gibbs free energy (ΔG^0), entropy (ΔS^0), and enthalpy (ΔH^0) changes:

$$K_d = \frac{q_e}{C_e} \quad (8)$$

$$\Delta G^0 = -RT \ln \rho_w K_d \quad (9)$$

$$\ln \rho_w K_d = -\frac{\Delta H^0}{RT} + \frac{\Delta S^0}{R} \quad (10)$$

In which K_d is the equilibrium constant (L mg⁻¹) and can be obtained from the intercept of Khan and Singh plots of $\ln q_e/C_e$ versus q_e (Krishna et al. 2000). ρ_w is the water density (mg L⁻¹). A straight line will occur using the plot of ($\ln(\rho_w K_d)$) versus ($1/T$), the slope of the straight line stands for ($-\Delta H^0/R$), and the intercept represents ($\Delta S^0/R$); Table 4 illustrated the calculated ΔH^0 and ΔS^0 .

The negative value of ΔG^0 indicates that nature of Pb²⁺ adsorption on synthetic Na-X zeolite is spontaneous. The values are -17.78, -19.24, and 20.41 kJ/mol at 298, 308,

Table 4 Thermodynamic parameters for Pb²⁺ adsorption on the synthetic zeolite

T (K)	ΔG^0 (kJ/mol)	ΔH^0 (kJ/mol)	ΔS^0 (J/(mol·K))
298	-17.78		
308	-19.24	21.5 kJ/mol	131.88
318	-20.41		

and 318 K, respectively. All the ΔG^0 values are lower than -15 kJ/mol but higher than -30 kJ/mol, which suggest that chemisorption rather than physisorption dominates the adsorption process (Al-zboon et al. 2011). With the increase of temperature, the decrease of ΔG^0 shows that the adsorption is more favorable at higher temperatures. This is well in agreement with the effect of temperature (Fig. 7). The positive value of ΔH^0 (21.5 kJ/mol) explains that the Pb²⁺ adsorption on the Na-X zeolite is an endothermic process (Li et al. 2015). The positive value of ΔS^0 (131.88 J/(mol·K)) not only shows that some structural changes at the solid-liquid interface exist but also indicates that the randomness increases with the removal of Pb²⁺ by Na-X zeolite (Saltali et al. 2007). This result also explains that chemical interactions (covalent and ionic) play the predominant roles in the adsorption of Pb²⁺ onto Na-X zeolite (Donat et al. 2005).

Comparison of various zeolite adsorbents

Comparative research for Pb²⁺ adsorption using the synthetic zeolite and other zeolite sorbents reported previously is revealed in Table 5. For example, Pb²⁺ adsorption capacity of Australia natural zeolite is 20.7 mg/g when 200 mg natural zeolite was added into 20 mg/L Pb²⁺ solution for 200 min at pH = 6 (Wang and Ariyanto 2007). So the Pb²⁺ adsorption capacity of the synthetic zeolite in this study is much higher than the Australia natural zeolite. Another instance, 100 mg of magnetic 4A zeolite could adsorb 100 mg/L of Pb²⁺ within 100 min at pH = 4 and the adsorption capacity was measured equal to about 100 mg/g (Xie et al. 2018). As another work, 10 mg of Na-Y zeolite was used for adsorption of 100 mg/L Pb²⁺ during 60 min at pH = 6, and adsorption capacity of 454.5 mg/g was achieved (Shariatnia and Bagherpour 2018). Hence, compared with the synthetic zeolite, Na-Y zeolite has almost the same adsorption capacity, but the time to reach equilibrium is longer. We can conclude that the synthetic zeolite exhibit satisfactory adsorption characteristics considering all parameters affecting the adsorption efficiency.

Table 5 Comparison of Pb²⁺ adsorption capacity between various zeolite adsorbents

Adsorbent	Dosage (mg)	Pb ²⁺ concentration (mg/L)	pH	Contact time (min)	Adsorption capacity (mg/g)	Reference
Faujasite (FAU)	400	800	3	150	143.3	Liu et al. 2016
Zeolite-Fe(0)	100	100	4	140	806	Kim et al. 2013
Nature zeolite	200	20	6	200	20.7	Wang and Ariyanto 2007
Magnetic 4A zeolite	100	100	4	100	about 100	Xie et al. 2018
Na-Y zeolite	10	100	6	60	454.5	Shariatinia and Bagherpour 2018
Magnetic zeolite	8	75	5.6	8	750	Khodadadi et al. 2017
ZSM-5 zeolite	200	20	3	10	20.1	Wang et al. 2015
Na-X zeolite	20	200	6	40	457	This work

Conclusion

Na-X zeolite was successfully synthesized from coal gangue via alkali fusion hydrothermal method. The synthetic process reveals the advantages of simple operation and easily obtained raw materials and has excellent potential to be implemented at a massive scale. CGP was directly melted with NaOH (mass ratio = 1:1.25) at 850 °C for 2 h, then ground for 5 min, stirred for 30 min and crystallized at 90 °C for 12 h under hydrothermal conditions. Compared with commercial zeolite, the product has the same microstructure and functional groups as industrial zeolite. For 50 mL 200 mg/L Pb²⁺ solution, when the optimal pH, contact time, temperature, and adsorbent dosage are 6, 40 min, 45 °C, and 0.02 g respectively, the adsorption capacity of synthetic zeolite reaches 457 mg/g, which is higher than some natural and other synthetic zeolites reported in previous literature. Kinetic studies show that Pb²⁺ adsorption followed pseudo-second-order model. Besides, Langmuir models are found to be better in the description of adsorption equilibrium data. It can be used as an excellent adsorbent for Pb²⁺ removal.

Funding information This work was financially supported by the Basic Research Program of Shanxi Province, China (No.201801D121267).

References

- Aldahri T, Behin J, Kazemian H, Rohani S (2016) Synthesis of zeolite Na-P from coal fly ash by thermo-sonochemical treatment. *Fuel* 182:494–501
- Al-harashsheh MS, Zboom KA, Al-makhadmeh L, Hararah M, Mahasneh M (2015) Fly ash based geopolymer for heavy metal removal : a case study on copper removal. *J Environ Chem Eng* 3:1669–1677
- Alijani H, Shariatinia Z (2017) Effective aqueous arsenic removal using zero valent iron doped MWCNT synthesized by in situ CVD method using natural α -Fe₂O₃ as a precursor. *Chemosphere* 171:502–511
- Alijani H, Hossein M, Shariatinia Z, Bayat M, Shemirani F (2014) A new approach for one step synthesis of magnetic carbon nanotubes / diatomite earth composite by chemical vapor deposition method : application for removal of lead ions. *Chem Eng J* 253:456–463
- Alijani H, Shariatinia Z, Aroujalian A (2015) Water assisted synthesis of MWCNTs over natural magnetic rock : an effective magnetic adsorbent with enhanced mercury (II) adsorption property. *Chem Eng J* 281:468–481
- Al-zboon K, Al-harashsheh MS, Bani F (2011) Fly ash-based geopolymer for Pb removal from aqueous solution. *J Hazard Mater* 188:414–421
- Barbosa R, Lapa N, Lopes H, Günther A, Dias D, Mendes B (2014) Biomass fly ashes as low-cost chemical agents for Pb removal from synthetic and industrial wastewaters. *J Colloid Interface Sci* 424:27–36
- Bhuiyan MAH, Parvez L, Islam MA, Dampare SB, Suzuki S (2010) Heavy metal pollution of coal mine-affected agricultural soils in the northern part of Bangladesh. *J Hazard Mater* 173:384–392
- Bortone I, Di Nardo A, Di Natale M, Erto A, Musmarra D, Santonastaso GF (2013) Remediation of an aquifer polluted with dissolved tetrachloroethylene by an array of wells filled with activated carbon. *J Hazard Mater* 260:914–920
- Donat R, Akdogan A, Erdem E, Cetisli H (2005) Thermodynamics of Pb²⁺ and Ni²⁺ adsorption onto natural bentonite from aqueous solutions. *J Colloid Interface Sci* 286:43–52
- Doyle AM, Alismael ZT, Albayati TM, Abbas AS (2017) High purity FAU-type zeolite catalysts from shale rock for biodiesel production. *Fuel* 199:394–402
- Faghihian H, Nourmoradi H, Shokouhi M (2012) Performance of silica aerogels modified with amino functional groups in Pb(II) and Cd(II) removal from aqueous solutions. *Pol J Chem Technol* 14:50–56
- Gao Y, Huang H, Tang W, Liu X, Yang X, Zhang J (2015) Preparation and characterization of a novel porous silicate material from coal gangue. *Microporous Mesoporous Mater* 217:210–218
- Gassowska M, Baranowska-Bosiacka I, Moczyłowska J, Tarnowski M, Pilutin A, Gutowska I, Struzynska L, Chlubek D, Adamczyk A (2016) Perinatal exposure to lead (Pb) promotes Tau phosphorylation in the rat brain in a GSK-3 β and CDK5 dependent manner: relevance to neurological disorders. *Toxicology* 349:17–28
- Haibin L, Zhenling L (2010) Resources, conservation and recycling recycling utilization patterns of coal mining waste in China. *Resources, Conserv. Recycl* 54:1331–1340
- Ibrahim HS, Jamil TS, Hegazy EZ (2010) Application of zeolite prepared from Egyptian kaolin for the removal of heavy metals : II. Isotherm models. *J Hazard Mater* 182:842–847
- Khodadadi M, Malekpour A, Ansaritabar M (2017) Removal of Pb(II) and Cu (II) from aqueous solutions by NaA zeolite coated magnetic nanoparticles and optimization of method using experimental design. *Microporous Mesoporous Mater* 248:256–265
- Kim SA, Kamala-Kannan S, Lee KJ, Park YJ, Shea PJ, Lee WH, Kim HM, Oh BT (2013) Removal of Pb(II) from aqueous solution by a zeolite-nanoscale zero-valent iron composite. *Chem Eng J* 217:54–60

- Krishna BS, Murty DSR, Prakash BJS (2000) Thermodynamics of chromium (VI) anionic species sorption onto surfactant-modified montmorillonite clay. *J Colloid Interface Sci* 229:230–236
- Lee M, Park J, Kam S, Lee C (2018) Chemosphere synthesis of Na-A zeolite from Jeju Island scoria using fusion / hydrothermal method. *Chemosphere* 207:203–208
- Li J, Wang J (2019) Comprehensive utilization and environmental risks of coal gangue: a review. *J Clean Prod* 239:117946
- Li M, Wang S, Luo W, Xia H, Gao Q, Zhou C (2015) Facile synthesis and in situ magnetization of carbon-decorated lignocellulose fiber for highly efficient removal of methylene blue. *J Chem Technol Biotechnol* 90:1124–1134
- Li X, Yan C, Luo W, Gao Q, Zhou Q, Liu C, Zhou S (2016) Exceptional cerium (III) adsorption performance of poly (acrylic acid) brushes-decorated attapulgite with abundant and highly accessible binding sites. *Chem Eng J* 284:333–342
- Liu C, Liu Y, Ma Q, He H (2010) Mesoporous transition alumina with uniform pore structure synthesized by alumisol spray pyrolysis. *Chem Eng J* 163:133–142
- Liu XD, Wang YP, Cui XM, He Y, Mao J (2013) Influence of synthesis parameters on NaA zeolite crystals. *Powder Technol* 243:184–193
- Liu Y, Yan C, Zhang Z, Wang H, Zhou S, Zhou W (2016) A comparative study on fly ash, geopolymer and faujasite block for Pb removal from aqueous solution. *Fuel* 185:181–189
- Liu Y, Yan C, Zhao J, Zhang Z, Wang H, Zhou S, Wu L (2018) Synthesis of zeolite P1 from fly ash under solvent-free conditions for ammonium removal from water. *J Clean Prod* 202:11–22
- Liu C, Xia J, Fan H, Li W, Zheng G, Ma G, Liang Y (2020) Ti leaching differences during acid leaching of coal gangue based on different thermal fields. *Waste Manag* 101:66–73
- Miyake M, Kimura Y, Ohashi T, Matsuda M (2008) Preparation of activated carbon – zeolite composite materials from coal fly ash. *Microporous Mesoporous Mater* 112:170–177
- Murayama N, Yamamoto H, Shibata J (2002) Mechanism of zeolite synthesis from coal fly ash by alkali hydrothermal reaction. *Int J Miner Process* 64:1–17
- Nekhunguni PM, Tavengwa NT, Tutu H (2017) Investigation of As (V) removal from acid mine drainage by iron (hydr) oxide modified zeolite. *J Environ Manag* 197:550–558
- Ojha K, Pradhan NC, Samanta AN (2004) Zeolite from fly ash: synthesis and characterization. *Bull Mater Sci* 27:555–564
- Pandey PK, Sharma SK, Sambi SS (2015) Removal of lead (II) from waste water on zeolite-NaX. *J Environ Chem Eng* 3:2604–2610
- Qian T, Li J (2015) Synthesis of Na-A zeolite from coal gangue with the in-situ crystallization technique. *Adv Powder Technol* 26:98–104
- Qin L, Gao X (2019) Properties of coal gangue-Portland cement mixture with carbonation. *Fuel* 245:1–12
- Reinoso D, Adrover M, Pedernera M (2018) Green synthesis of nanocrystalline faujasite zeolite. *Ultrason Sonochem* 42:303–309
- Ren H, Jiang J, Wu D, Gao Z (2016) Selective adsorption of Pb (II) and Cr (VI) by surfactant-modified and unmodified natural zeolites: a comparative study on kinetics, equilibrium, and mechanism. *Water Air Soil Pollut* 227:3–11
- Reynolds JG, Coronado PR, Hrubesh LW (2001) Hydrophobic aerogels for oil-spill cleanup – synthesis and characterization. *J Non-Cryst Solids* 292:127–137
- Saltali K, Sarı A, Aydın M (2007) Removal of ammonium ion from aqueous solution by natural Turkish (Yıldızeli) zeolite for environmental quality. *J Hazard Mater* 141:258–263
- Shariatnia Z, Bagherpour A (2018) Synthesis of zeolite NaY and its nanocomposites with chitosan as adsorbents for lead (II) removal from aqueous solution. *Powder Technol* 338:744–763
- Sivalingam S, Sen S (2018) Rapid ultrasound assisted hydrothermal synthesis of highly pure nanozeolite X from fly ash for efficient treatment of industrial effluent. *Chemosphere* 210:816–823
- Wang S, Ariyanto E (2007) Competitive adsorption of malachite green and Pb ions on natural zeolite. *J Colloid Interface Sci* 314:25–31
- Wang C, Li J, Wang L, Sun X (2008) Influence of NaOH concentrations on synthesis of pure-form zeolite A from fly ash using two-stage method. *J Hazard Mater* 155:58–64
- Wang X, Shao D, Hou G, Wang X, Alsaedi A, Ahmad B (2015) Uptake of Pb(II) and U (VI) ions from aqueous solutions by the ZSM-5 zeolite adsorption percent (%). *J Mol Liq* 207:338–342
- Wang J, Qin Q, Hu S, Wu K (2016) A concrete material with waste coal gangue and fly ash used for farmland drainage in high groundwater level areas. *J Clean Prod* 112:631–638
- Wei P, Zhu X, Wang Y, Chu W, Xie S, Yang Z, Liu X, Li X, Xu L (2019) Rapid synthesis of ferrierite zeolite through microwave assisted organic template free route. *Microporous Mesoporous Mater* 279:220–227
- Xie W, Zhou F, Bi X, Chen D, Li J, Sun S, Liu J, Chen X (2018) Accelerated crystallization of magnetic 4A-zeolite synthesized from red mud for application in removal of mixed heavy metal ions. *J Hazard Mater* 358:441–449
- Yang T, Han C, Liu H, Yang L, Liu D, Tang J, Luo Y (2019a) Synthesis of Na-X zeolite from low aluminum coal fly ash: characterization and high efficient As (V) removal. *Adv Powder Technol* 30:199–206
- Yang L, Qian X, Yuan P, Bai H, Miki T, Men F, Li H, Nagasaka T (2019b) Green synthesis of zeolite 4A using fly ash fused with synergism of NaOH and Na₂CO₃. *J Clean Prod* 212:250–260
- Zanin E, Scapinello J, De Oliveira M, Maria J, De Mello M, Antonio M, Oliveira JV, Dal J (2016) Adsorption of heavy metals from wastewater graphic industry using clinoptilolite zeolite as adsorbent. *Process Saf Environ Prot* 105:194–200
- Zhang X, Tang D, Zhang M, Yang R (2013) Synthesis of NaX zeolite: influence of crystallization time, temperature and batch molar ratio SiO₂/Al₂O₃ on the particulate properties of zeolite crystals. *Powder Technol* 235:322–328
- Zhang H, Gu L, Zhang L (2017) Removal of aqueous Pb(II) by adsorption on Al₂O₃-pillared layered MnO₂. *Appl Surf Sci* 406:330–338
- Zhao Y, Zhang B, Zhang X, Wang J, Liu J, Chen R (2010) Preparation of highly ordered cubic NaA zeolite from halloysite mineral for adsorption of ammonium ions. *J Hazard Mater* 178:658–664
- Zhou C, Liu G, Wu S, Kwan P, Lam S (2014) The environmental characteristics of usage of coal gangue in bricking-making: a case study at Huainan, China. *Chemosphere* 95:274–280
- Zhou J, Zheng F, Li H, Wang J, Bu N, Hu P, Gao J (2020) Optimization of post-treatment variables to produce hierarchical porous zeolites from coal gangue to enhance adsorption performance. *Chem Eng J* 381:122698

Publisher's note Springer Nature remains neutral with regard to jurisdictional claims in published maps and institutional affiliations.